Inventory of natural processes with nautical charts, real-time kinematic global navigation satellite systems (RTK-GNSS), and unmanned aerial vehicle (UAV), Trindade Island, Brazil

Fernanda Avelar Santos[1]* , Maria Cristina de Souza[1] , Lázaro Valentin Zuquette[2] , Rodolfo José Angulo[1] , Maria Luiza Correa da Camara Rosa[3] , Adriana Ahrendt Talamini[4] , Carolina Almeida Figueiredo[5]

Abstract

The volcanic Trindade Island is a remote Brazilian offshore territory in the South Atlantic, located ca. 1.140 kilometers east of the southeast coast of Brazil. The island's permanent exposure to geological hazards requires assessment. However, the lack of erosion and landslides temporal data impedes predictive geohazard analyses. Therefore, we compiled pre-existing data from nautical charts and surveyed the surface terrain on Trindade Island to generate Digital Terrain Models (DTMs) and comparative accuracy analyses. The DTM based on pre-existing data shows the lowest accuracy (root mean square error – RMSE: 12.3 m) yet is adequate for regional studies. In contrast, the DTM developed from real-time kinematic global navigation satellite systems (RTK-GNSS) has the highest vertical accuracy (RMSE: 0.48 m), but spatial variability of ground elements was underestimated and limited to meter-sized (and larger) elements. The DTM obtained using the unmanned aerial vehicle (UAV) with ground control points (GCP), on the other hand, presented lower accuracy (RMSE: 2.37 m) than the RTK-GNSS model but still allowed observation of centimetric (and larger) ground features. For geohazard assessment on Trindade Island, models that allow fine-scale studies are needed. A UAV with GCP provides such standards and proved to be the most viable option in remote and complex sites as well. Hence, this study, the first to allow multi-temporal analysis of geohazard assessment on Trindade Island, offers a viable solution for similar analyses in other remote locations.

KEYWORDS: geotechnology; geohazard assessment; digital terrain model; volcanic landscape; South Atlantic Ocean.

INTRODUCTION

Geotechnology is a scientific approach that comprises technologies linked to survey, database archiving, processing, and development of applications using geo-referenced data (Souza Filho and Crósta 2003). The geotechnologies applied in the earth surface data survey are efficient tools for monitoring and mapping erosive and gravitational processes in geohazards assessments (Hashemi-Beni *et al.* 2018, Guenzi *et al.* 2019, Hu *et al.* 2019, Tan *et al.* 2021). These depend on the ability to accurately measure changes in the landscape according to specific rock or soil processes (Wernette *et al.* 2020). The geohazards can be evaluated in detail using a digital terrain model (DTM) generated from topographic maps, real-time kinematic global navigation satellite systems (RTK-GNSS), and an unmanned aerial vehicle (UAV) (e.g., Evans and Lindsay 2010, Muço *et al.* 2012, Tannant 2015, Mohamad *et al.* 2019, Mohammadi *et al.* 2020, Chaudhry *et al.* 2021).

Oceanic volcanic islands (e.g., Santos *et al.* 2019), like Trindade Island, present adversities in field acquisition not only due to their geographical remoteness but also on account of numerous landforms (e.g., plugs, necks, dikes, and scoria cones), rocks with distinct erodibility (e.g., basaltic lava flows interspersed by pyroclastic deposits), climate (e.g., strong winds, storms), and vegetation, which condition a rugged relief and heterogeneous landscape. These natural settings represent challenges for the survey and affect the accuracy of digital surface models through unrealistic altitudes and significant gaps. Deng *et al.* (2019) reported that these limitations result in the lack of a global high-resolution DTM of the volcanic environment, thus limiting the accuracy of a detailed hazard assessment in these regions (Global Volcanism Program 2013). Another difficulty

[1]Laboratório de Estudos Costeiros, Programa de Pós-Graduação em Geologia, Universidade Federal do Paraná – Curitiba (PR), Brazil. E-mails: fernanda.avelars@gmail.com, cristinasouza2527@gmail.com, fitoangulo@gmail.com

[2]Departamento de Geotecnia, Escola de Engenharia de São Carlos, Universidade de São Paulo – São Paulo (SP), Brazil. E-mail: lazarus1@sc.usp.br

[3]Departamento de Geodésia, Instituto de Geociências, Universidade Federal do Rio Grande do Sul – Porto Alegre (RS), Brazil. E-mail: luiza.camara@ufrgs.br

[4]Departamento de Geologia, Universidade Federal do Paraná – Curitiba (PR), Brazil. E-mail: adratal@gmail.com

[5]Departamento de Geologia, Universidade Federal do Rio de Janeiro – Rio de Janeiro (RJ), Brazil. E-mail: carol.almeidaf56@gmail.com

*Corresponding author.

for geohazards studies on Trindade Island is the lack of temporal data since the small-scale resolution of the available remote sensing images hinders the visualization of terrain features in detail.

In this sense, our goal is to produce a comparative analysis of the quality and accuracy of digital models generated from pre-existing data, RTK-GNSS, and UAV for relief characterization and inventory of natural processes on a fine scale. Thereby, we enable the first multi-temporal database for assessing and monitoring the evolution of erosional and depositional features for future geohazards prediction analyses on Trindade Island. Furthermore, we contribute to the attainment of relief data in remote and difficult-to-access regions with rugged terrain with minimal human resources and field materials, and relatively low cost to perform.

STUDY AREA SETTINGS

The study area, approximately 2 km², 20°30'40" S latitude and 29°18'40" W longitude, is located upstream of the Trindade Island's anthropogenic activities and constructions (Fig. 1). Such area comprises active erosive processes and slopes with the talus and debris flow deposits, with the possibility of instability processes (Fig. 2), classified as geohazards according to the definition by UNESCO (2019). The crucial issues to be considered before applying field techniques for geological hazards studies are summarized below. Such issues refer to geology (relief and the study object), geomorphology (essential for planning the field walk), and environmental settings (vegetation size and climatic conditions that are essential for the use of technologies in the field).
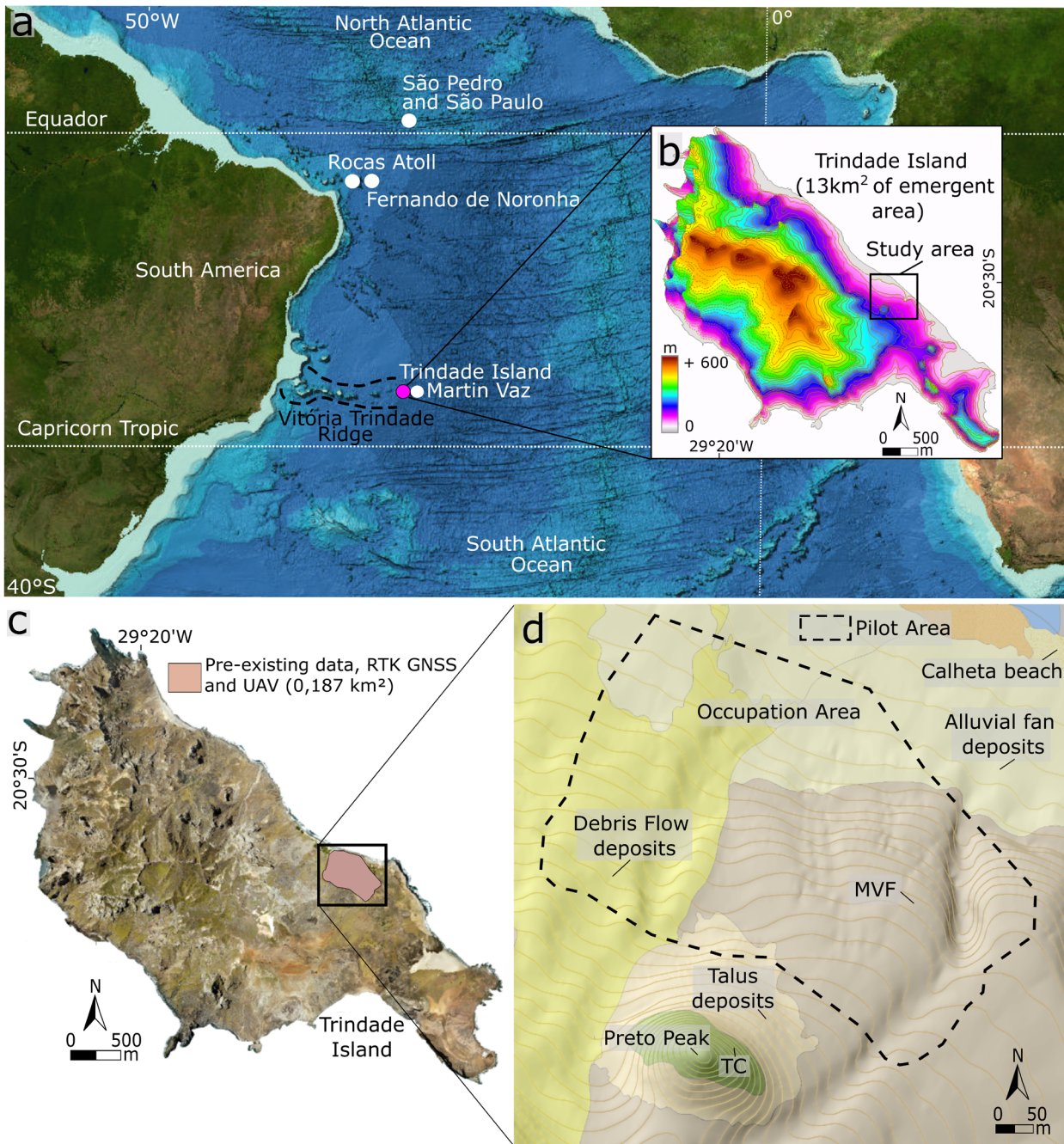
TC: Trindade Complex; MVF: Morro Vermelho Formation.
Figure 1. Location of the study site: (A) South Atlantic Brazilian oceanic islands between 0.9°N and 20.47°S, the location of Trindade Island (latitude 20.5°S, longitude 29.3°W) at the easternmost of the Vitória-Trindade Ridge (GEBCO Image); (B) the topography model of Trindade Island (vertical exaggeration: 2) produced from contour lines of the nautical chart (Marinha do Brasil 2011); (C) aerial image by the Brazilian Navy (Marinha do Brasil 2011) with the areas covered through different acquisition methods; (D) local geological map of the study area.
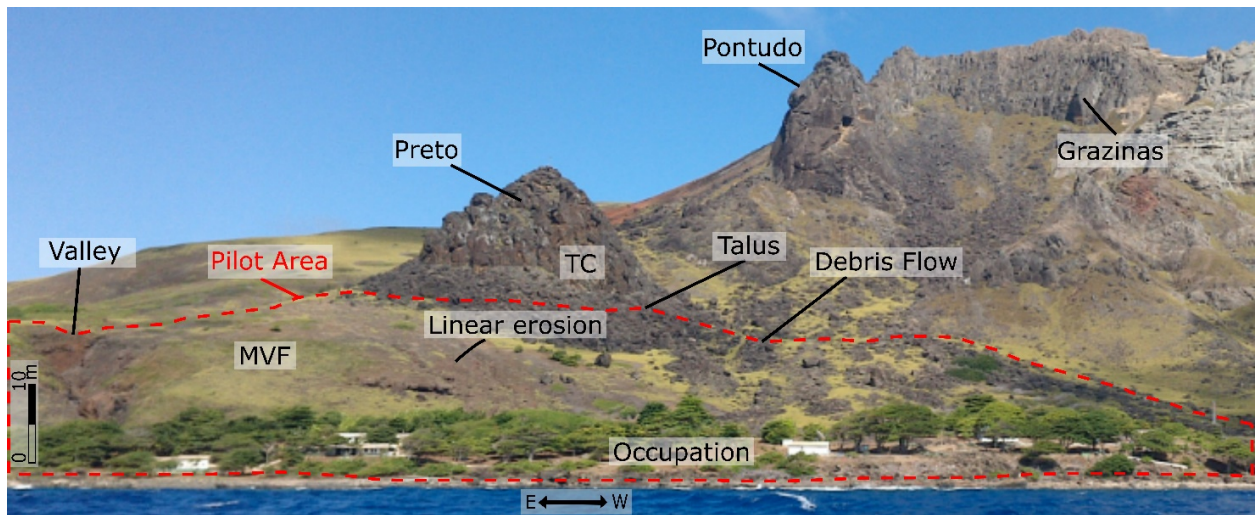
Figure 2. The study area (delimited by the red dashed line) indicating occupation downstream, MVF outcropping with the prevalence of linear erosive features, and outflow of the erosive valley. Also, the important volcanic landforms from the Trindade Complex (Preto, Pontudo, and Grazinas peaks) that supply the large boulder to debris flow and talus deposits are indicated.

Almeida (1961) delimited the island into five units composed of lava flows, dikes and necks, and pyroclastic deposits. However, quaternary deposits (e.g., debris flow, talus, alluvial fans) cover most of the terrain surface in the study area (Fig. 1D). The Trindade Complex (TC), the basement of the island, occurs at Preto Peak and is covered by debris flow deposits in the western portion of the study area. Also, the Morro Vermelho Formation (MVF) occurs in the eastern portion, composed of lava flows and pyroclastic deposits.

Most of the Trindade Island terrain presents steeply sloping hills surrounded by talus slope deposits, alluvial fans/cones (Almeida 1961, 2002, Angulo *et al.* 2018), and debris flow deposits. Gully erosion occurs in the eastern part of the study area, with a maximum depth of 17 m near the anthropogenic infrastructure (Fig. 2). The western portion consists of deposits of large debris flow, with boulders up to 30 m in diameter, derived from volcanic necks and dome from the TC, named: Preto Peak, Pontudo Peak, and Grazinas Peak, respectively (Fig. 2).

Trindade Island is under the Tropical Oceanic climate that occurs in the South Atlantic Subtropical Anticyclone region (Cavalcanti *et al.* 2009). It consists of elevated temperatures between 22.9 and 27.7°C, high humidity levels due to ocean evaporation, annual average rainfall of 921 mm, and monthly averages with a minimum of 64 mm and a maximum of 215 mm (Pedroso *et al.* 2017). According to Pedroso *et al.* (2017), such weather conditions make the island vulnerable to extratropical cyclones, instability lines, and cold fronts. Moreover, the study area has shrub vegetation (e.g., Silva and Alves 2017) and large exotic trees that exceed 3 m in height (Fig. 2).

MATERIALS AND METHODS

As Trindade Island is a restricted and remote area, the activities performed in the study area present difficulties. Transportation, for example, is pre-defined a few times a year by the Brazilian government with programmed residence time. Therefore, the research strategy employed is crucial, especially regarding fieldwork planning. In this sense, the fieldwork took place in 2018 and 2019. We used the pieces of equipment according to the availability of the Coastal Studies Laboratory of the Universidade Federal do Paraná. In the next section, the methodology steps followed in the present study were summarized.

Data acquisition and processing

Pre-existent data

The topographic base available on Trindade Island refers to the nautical chart, data collected by the Brazilian Navy until 1968 on a 1:15,000 scale (contour lines: 20 m equidistance) (Fig. 3A). However, the Suppl. Mat. (also from the Brazilian Navy) that illustrates access to the occupation area and topography (contour lines: 2 m equidistance) has a 1:5,000 scale (Fig. 3B). Therefore, both cartographic bases display an altimetric data gap (see Fig. 3). In the present study, such contours were digitized and merged to generate the elevation model. We used the ArcGIS 10.6.1 software to interpolate contour lines with Topo to Raster method (with 3 m input cell size, determined from the software's algorithm). The photogrammetric data (30 cm resolution) from 2011 was provided by the Brazilian Navy (see Ramos *et al.* 2008); however, altimetric data is lacking.

Global navigation satellite system

We used the single-base method for RTK-GNSS positioning, which consists of one master station (with well-known coordinates), and a rover device for measuring the points (with unknown coordinates) in real-time (Dabove *et al.* 2019) (Fig. 4). It is an attractive technique since signals are available in all-weather conditions and are continuous. Therefore, the method represents a near-real-time sensing tool (Jin *et al.* 2014, Mendez-Astudillo *et al.* 2021), which plays a crucial role in far-off sites such as Trindade Island.

The equipment model used was Stonex Plus 8, and the acquisition software was SurvCe. The horizontal and vertical accuracies were specified at 0.014 m and 0.039 m, respectively. The base transmits observation corrections to a rover receiver

via UHF radio in the field, with a distance of 470 m to the far-thest point. No level reference was defined, so we determined the base coordinates in a static survey of 600 readings. Next, we surveyed the rover points using the static-kinematic method (stop and go) along the surface on which trekking was viable.

The post-processing step consisted in converting geometric (or ellipsoidal) altitudes into orthometric ones. The ellipsoidal height (h) corresponds to the RTK-GNSS surveying, and we calculated the orthometric height through the mean sea level (e.g., Mohamad *et al.* 2019, Abdalla and Mustafa 2021). We performed the conversion from waterline measurements in which the tidal level determined the orthometric altitude to fill the gap of a high-resolution geoidal model for Trindade Island. The value measured was 0.6 m (June 20, 2019, at 3:30 p.m.). The tide level was based on the 2019 tide table of the

Brazilian Navy for Trindade Island (Coordinated Universal Time - UTC: +02). We used the Equation 1:

$$H = h - N \text{ at all points acquired} \tag{1}$$

Where:
N = the geoid height.

We used ArcGIS 10.6.1 software to interpolate the acquired and corrected points and create a surface model. The sample data around the study area boundary were extrapolated at the interpolation step, totalizing 11,270 points. Due to the density and high resolution of the data acquired in the field, the cell size chosen for the digital models of the terrain sur-face was 2 m, a value determined by the software's algorithm.
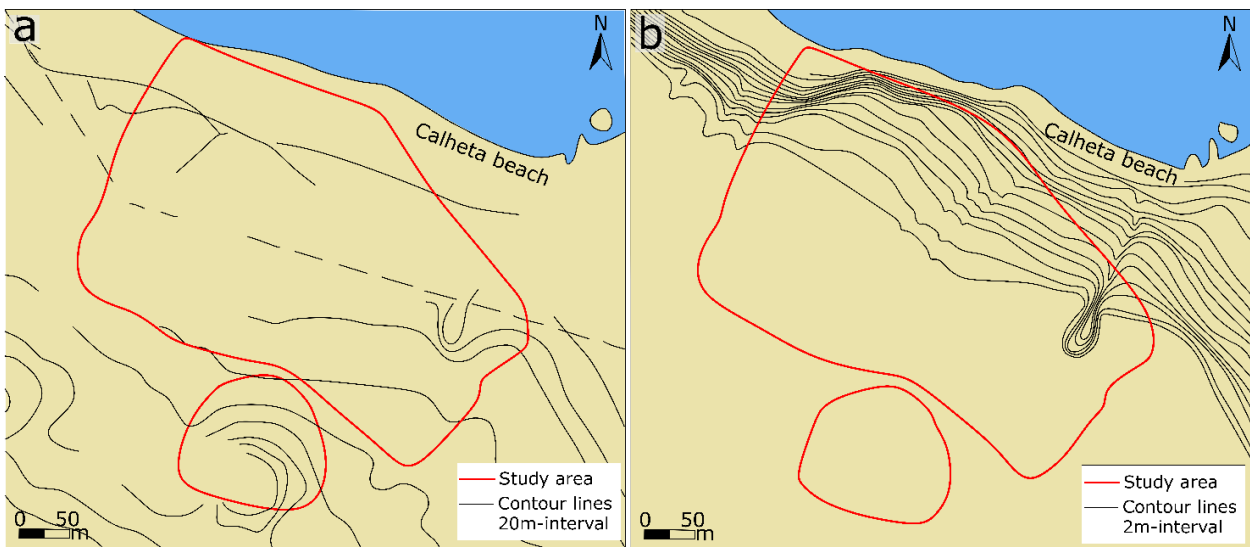
Source: modified from DHN (1971).
Figure 3. Pre-existing topographic data of the study area (delimited by the red line) on Trindade Island: (A) nautical chart (1:15,000 scale) and (B) supplementary nautical chart in the occupation area (1: 5,000 scale). Note the lack of topographic data in both data sources.
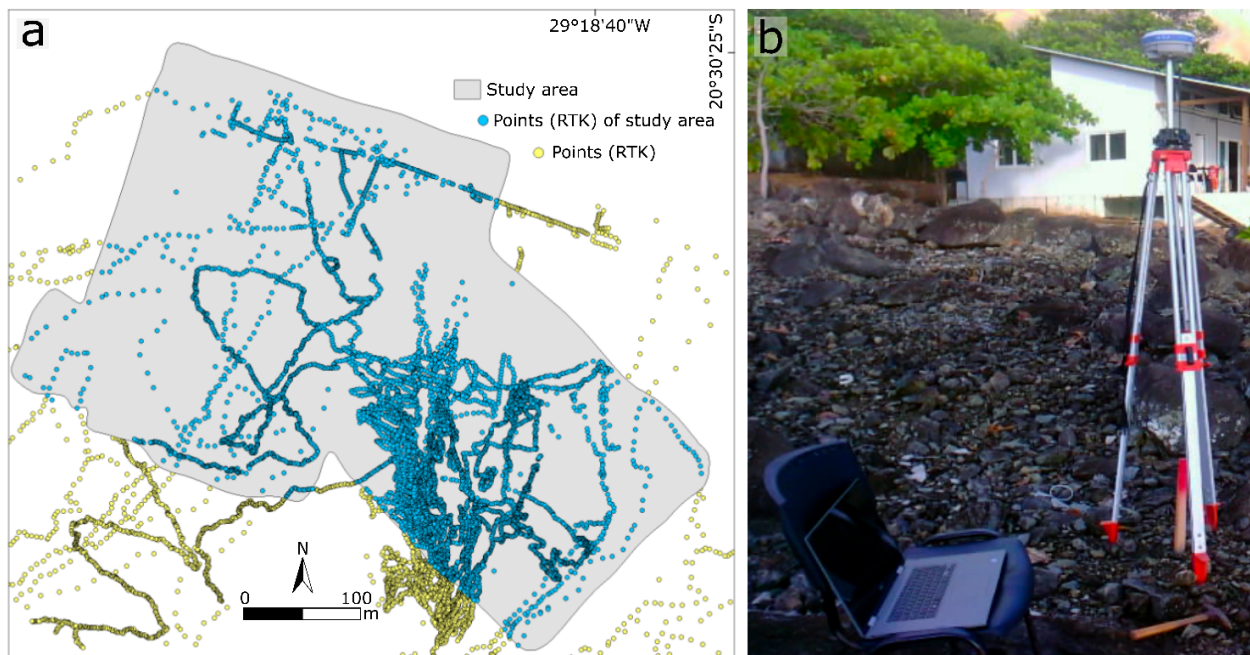

Figure 4. RTK-GNSS surveying: (A) density of points acquired in the study area; (B) master station of single-base RTK-GNSS positioning to determine coordinates in a static survey.

We produced DTMs with nine elevation classes according to six spatial interpolation methods. We compared the vertical accuracy of DTMs with checkpoints and spatial accuracy with field observations (see Suppl. Mat.), and evaluated the most appropriate model to represent the terrain (e.g., Aguilar *et al.* 2005).

We used and compared the following techniques described by Childs (2004):

- Triangulated Irregular Network (TIN): a set of irregularly spaced data points that are connected by edges that form contiguous, nonoverlapping triangles and create a continuous surface to produce terrain models;
- Inverse Distance Weighted (IDW): the cell values are determined using a linear-weighted combination set of sample points, in which the weight assigned is a function of the distance of an input point from the output cell location;
- Kriging: it fits a function of points within a specified radius to determine the output value for each location and assumes that the distance or direction between the sample points reflects a spatial correlation;
- Topo to Raster: designed to work with contour inputs, it uses an interactive finite difference interpolation technique that optimizes the computational efficiency of local interpolation;
- Natural Neighbor: linear-weighted method (IDW-like interpolation), but the local coordinates define the amount of influence any scatter point will have on output cells;
- Spline: through a mathematical function, the values are estimated and enable a smooth surface that passes exactly on input points, and there are two variations (regularized and tension).

Unmanned aerial vehicle photogrammetry

An UAV is a standard platform for photogrammetric data capture (e.g., Haala *et al.* 2011, Uysal *et al.* 2015). We borrowed the term UAV from computer science and artificial intelligence communities. We utilized Phantom 3 Advanced – DJI UAV equipped with an FC300S camera with a focal length of 3.61 mm, pixel size $1.56 \times 1.56\,\mu$m, and image size (pixels) 4,000 × 3,000, and used the PIX4D Capture software for flight surveys.

However, the GPS of the UAV onboard navigation system (resolution: 10 m) is inappropriate for detailed studies. In this sense, RTK-GNSS data are crucial for the geo-referencing step (Mohamad *et al.* 2019). Before image acquisition, we scattered 14 coded targets on the studied surface and selected two anthropogenic structures, measured with RTK-GNSS, to improve the precision and accuracy of UAV photogrammetry. Autonomous flight data acquisition recorded an area of 0.2 km² within six flight stripes. Each flight had approximately five control points. However, winds above 16 knots made the flight survey to the Calheta beach area impossible on the last day of acquisition. Figure 5 shows the details of field acquisition.

A 3D flight planning provided a constant flight altitude of about 20 m above the ground level from the take-off position. The survey orientation followed areas with similar altimetry to maintain a relative flight height. We programmed a coverage of 80% along the flight lines and 60% between flights. The length of each flight was 20 minutes according to the battery autonomy. However, the natural conditions of Trindade Island led to variations in altitude and in the flight directions previously determined. We summarized information regarding survey data and camera calibration in the supplementary material.

The images were processed using the Agisoft Photoscan software with Structure from Motion-Multi View Stereo (SfM-MVS) algorithm and GCP procedure (Fig. 6). We chose setting options according to the computational resources (16 GB of Random-Access Memory-RAM) and the particularities of the Trindade Island landscape. The workflow required about 50 hours and 40 minutes to process 2,328 photos (12,3 GB), and the steps that required the longest processing time were building dense clouds (30 h) and texturing (11 h).
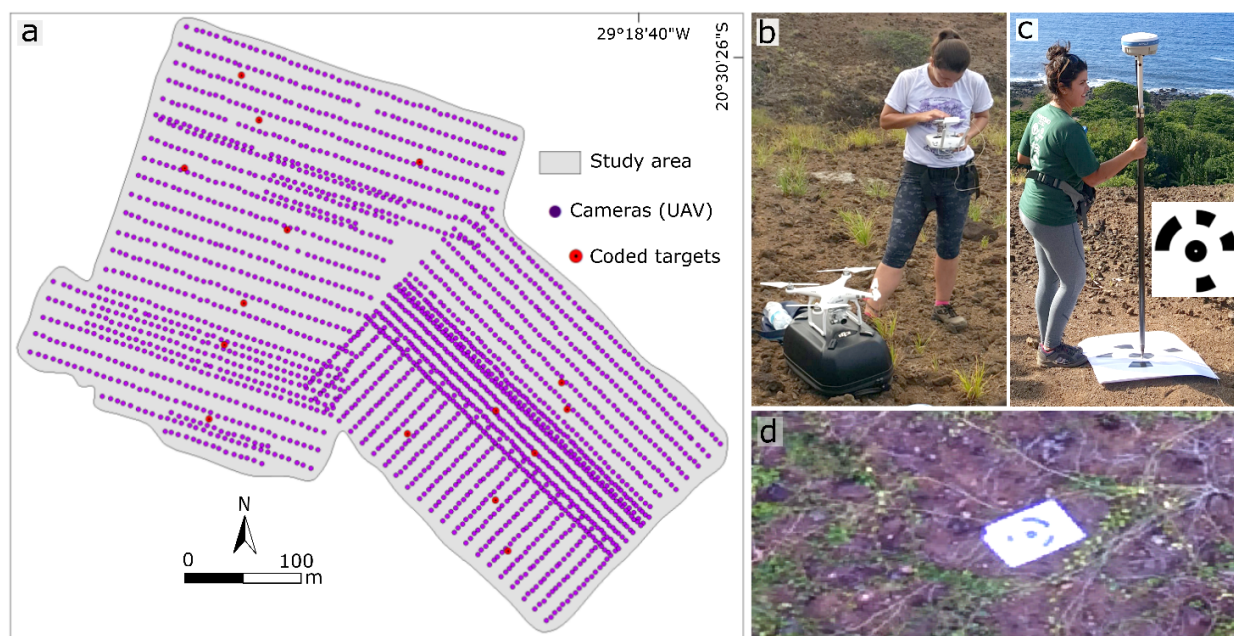

Figure 5. UAV and GNSS vertical data surveying: (A) density of points acquired; (B) the quadcopter UAV equipped with an autonomous control system ready for launch; (C) control points (encoded target) measured using RTK-GNSS (total: 14 targets); (D) aerial view of the encoded target.

Accuracy assessment

We carried out a vertical and spatial variability accuracy assessment of the DTMs using the techniques described above to compare the quality of the data generated. First, we validated the vertical accuracy of the DTMs via field-based measurements on bare surfaces. For this purpose, 20 checkpoints measured by RTK-GNSS were selected (Suppl. Mat. Table 4). We generated the following standard accuracy statistics: mean absolute error (MAE), root mean square error (RMSE), and RMSE/MAE ratio as a complementary result (e.g., Karunasingha 2022). The second approach analyzed spatial variability according to the erosional and gravitational features observed on-field and in 3D models.

## RESULTS

RTK-GNSS: spatial interpolation algorithm

Although the RTK-GNSS equipment had a high collection accuracy, it is expected that the DTM presents lower accuracy due to irregular sampling distribution resulting from the complex landscape. Therefore, it was helpful to analyze which interpolation method provided the finest DTM for surface representation. We compared six interpolation algorithms (Fig. 7) enabled in the ArcGIS software from this irregular data. In addition, we compared the vertical accuracy of the DTMs generated with checkpoints (Suppl. Mat. Table 5) and spatial accuracy with field observations, such as terrain roughness in the eastern portion, three main drainages, and lower slope in the area near the coastal region (between altitudes of approximately 0 and 20 m).

The spline method presented the highest vertical accuracy with an RMSE of 0.48 m. The TIN showed the second-highest accuracy with an RMSE of 1.68. The natural neighbor, IDW, and topo to raster methods provided an RMSE of 1.71, 2.01, and 2.13 m, respectively. The kriging method showed the lowest accuracy with an RMSE of 2.2 m. Regarding the spatial variability of terrain features, all interpolation methods presented the main linear features and had a similar range of altitudes in each class. However, the DTM of the spline method presented a smoothly varying surface, minimizing overall surface curvatures, and predicting ridges and valleys. Therefore, we selected the MDT from the spline method for comparative analyses between different data sources.

Digital terrain models

DTMs were processed from different databases applied to relief characterization and inventory of natural processes
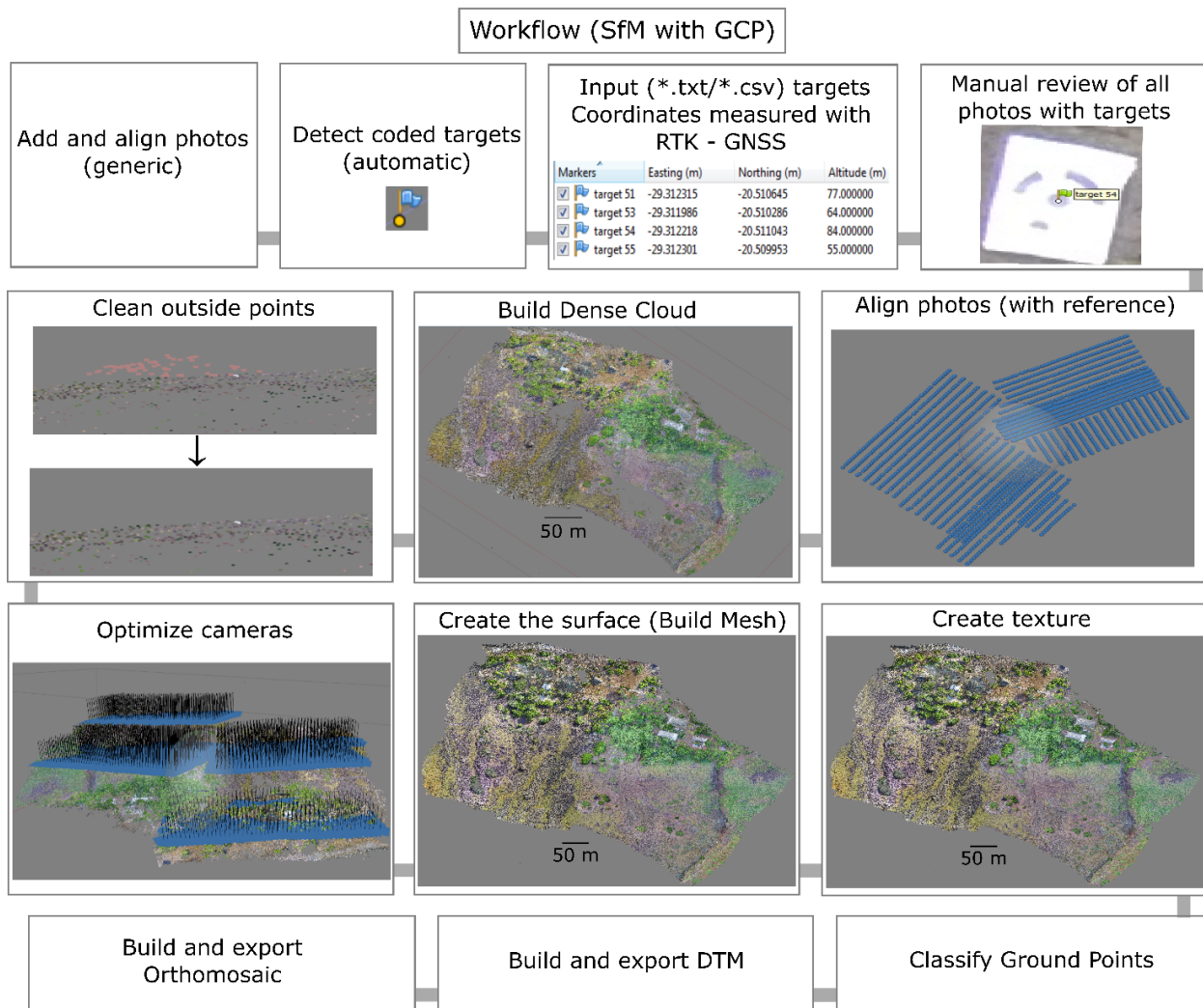
SfM: Structure from Motion; GCP: Ground Control Points; DTM: Digital Terrain Model.
Figure 6. The workflow presents a multi-step process to generate orthophoto images and models through a UAV survey.

(Fig. 8, Table 1). The attributes considered in the description were erosion (e.g., rill, gully) and gravitational features (e.g., landslides, deposits of debris, and boulders), drainages, geological contacts, anthropogenic infrastructure, and vegetation. The DTM based on pre-existing data from 1967 had a raster resolution of 3 m (Fig. 8A) and enabled the visualization of the most prominent linear features of the terrain. It consisted of three erosive drainages in the central and eastern portions of the area, with width variation between 5 m (watercourse) and 20 m (deep erosive valley), and presented a minimum length of 310 m.

The DTM based on RTK-GNSS data processing had a raster resolution of 2 m (Fig. 8B). The altitude ranged from 0 to 93 m. The DTM highlighted the mean erosive and gravitational ground features, such as prominent linear erosive features (length: 8 to 228 m) in the southeast portion of the study area, the boundaries of the large debris flow deposits in the western portion (the measured volume ranged between 78,349-154,461 m³), and the boundary of outflow of the deep valley on the eastern portion (volume below 118,137 m³). The DTM obtained through UAV photogrammetry had a raster resolution of 7.15 cm (Fig. 8C). The difference between the highest and lowest point was 92 m. Landform analysis detected significant erosion on the southeast portion, and dynamic slope mass movements occurred with well-defined scars in the eastern boundary. The UAV-DTM also presented large debris flow deposits in the western portion (measured volume between 693 to 9,089 m³), a significant number of linear erosions (0.2 to 320 m length) in the southeast part, and a precise outflow boundary of a deep valley on the eastern area (volume below 27,292 m³).

Comparative analyses of pre-existing data, RTK GNSS, and UAV DTMs

Vertical accuracy

We measured the discrepancy between the DTMs via 20 independent reference points scattered in the pilot area (Table 2). According to the comparison results, the DTM produced from RTK-GNSS had the highest vertical accuracy in bare terrain conditions, with an RMSE of 0.48 m. On the other hand, the UAV-GNSS also provided acceptable accuracy, with an RMSE of 2.37 m. The DTM from pre-existing data provided the lowest accuracy with an RMSE of 12.3 m.

In the DTM based on pre-existing data, the highest discrepancies compared with checkpoints occurred where a topographic data gap was observed in the nautical charts (see Fig. 3). The discrepancies in the DTM based on RTK-GNSS were generally low (< 1 m). However, the highest (> 2 m) discrepancies were located in the slopes downstream, with high vegetation density and buildings. In the DTM from UAV-GNSS, the highest disparities referred to the boundaries of the area surveyed and the northeast region (slope downstream), where a lack of image overlapping occurred (see Fig. 5A) that coincided with the tallest trees zone. Like the RTK-GNSS, the UAV-GNSS also presented the lowest discrepancies in bare terrain, referring to upstream portions of the slopes.

Also, for the vertical accuracy assessment, two profiles — 600 m and 550 m in length — were evaluated on the same portions for each technique (Fig. 9). A topographic data gap in the DTM from the nautical charts was evident in profile A-A' (Fig. 9), in which the software randomly performed the topographic profile between the distance of 0–450 m due to
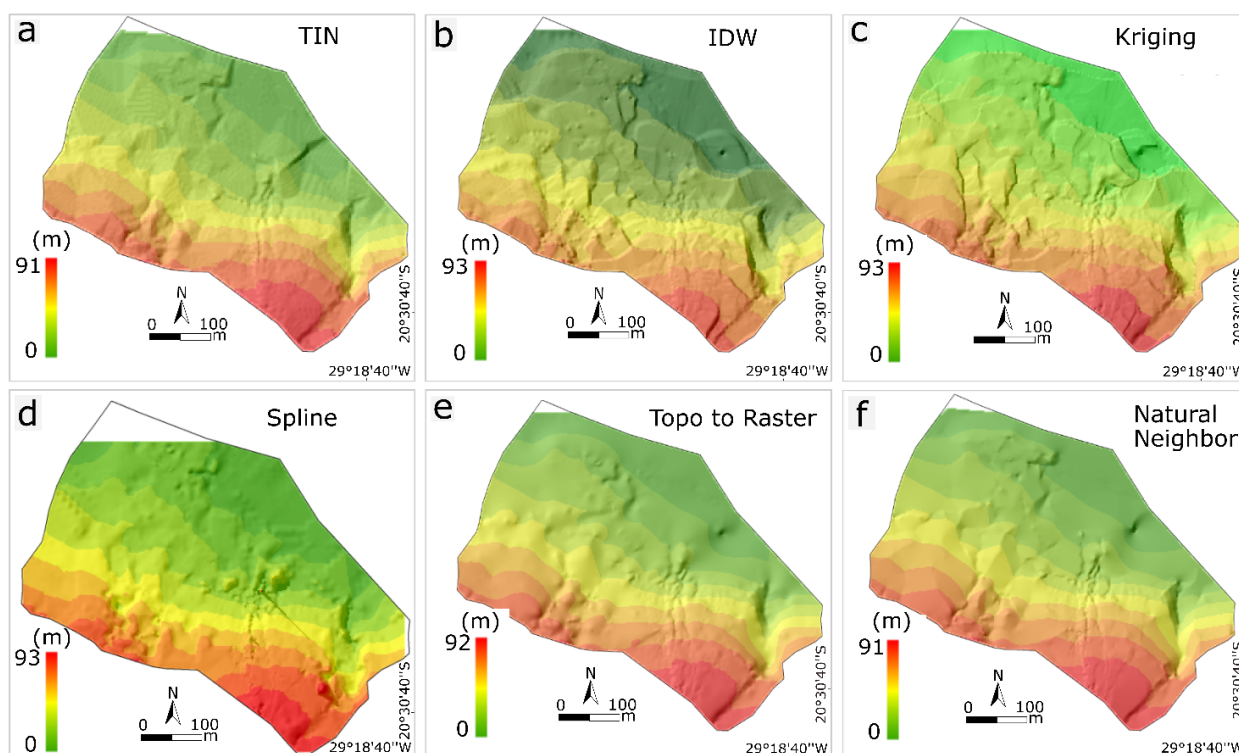

Figure 7. Spatial interpolation algorithm employed with the ArcGIS software to evaluate the most appropriate model to portray the study area compared to field-based measurements: (A) Triangulated Irregular Network (TIN); (B) Inverse Distance Weighted (IDW); (C) Kriging; (D) Spline; (E) Topo to Raster; (F) Natural Neighbor interpolation.

the lack of altitude data. However, despite the pre-existing data error being higher than RTK and UAV (Table 2), the three techniques provided similar results in profiles B-B'.

The RTK-GNSS profiles revealed the main abrupt relief changes in these lands compared to field-based measurements. These allowed us to correlate the significant relief breaks with

differential erosion of the MVF, especially in the outflow of the valley (east area) where large-scale landslides occurred. The elevation profiles of the UAV-DTM elucidated the rugged terrain in detail, relief breaks (valley, linear erosions, streams), and landform prominences caused by debris flow deposition. Moreover, the profiles also incorporated obstacles — besides
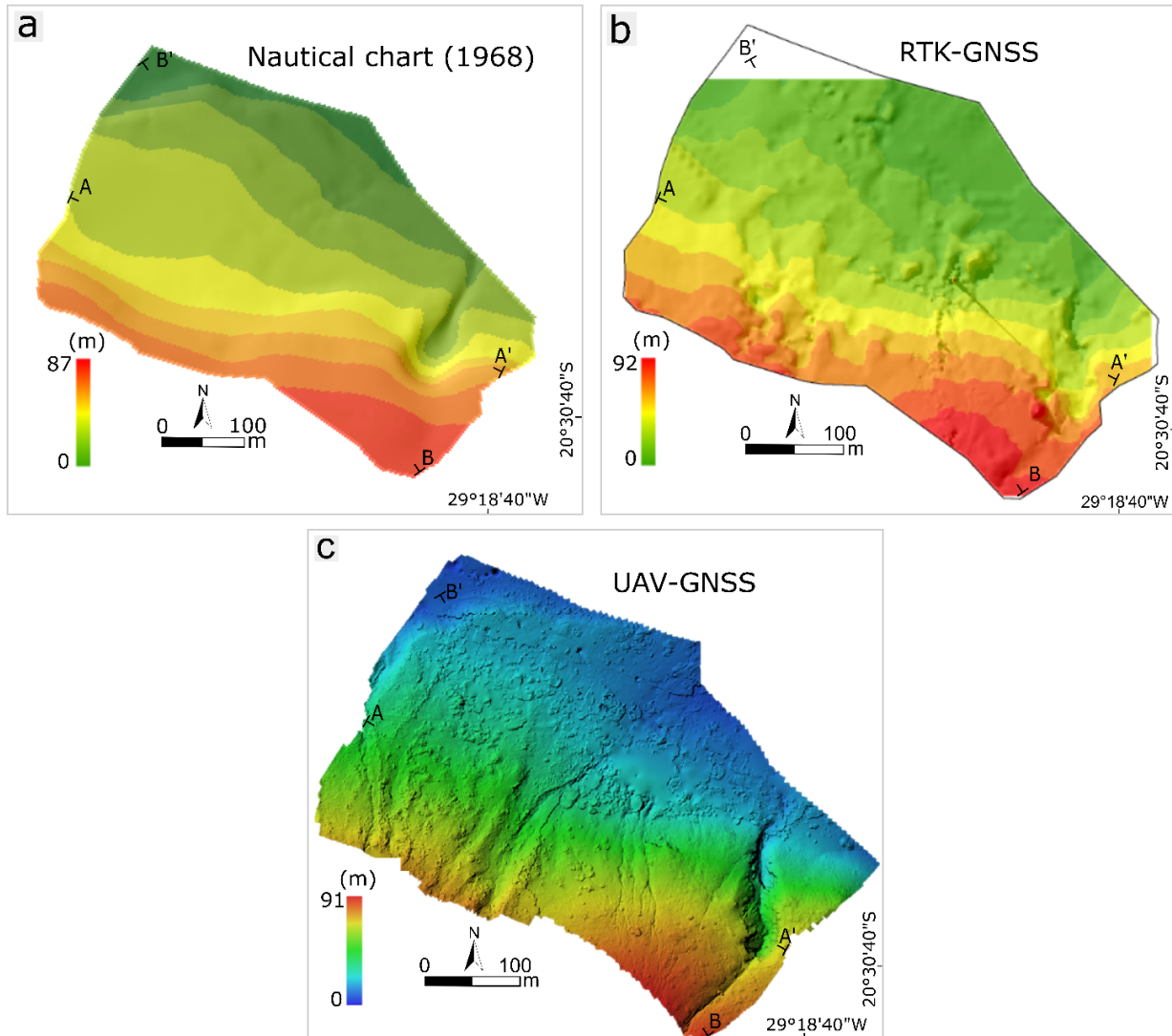

Figure 8. DTMs from different metadata: (A) contour lines data extracted from nautical charts (1968): model, performed by GIS software, overgeneralized the ground surface; (B) RTK-GNSS: model, performed by GIS software through spline-based interpolation method, highlighted the most prominent terrain roughness; (C) UAV photogrammetry with GNSS vertical data: model, performed by the Agisoft software, showed rich detail of the terrain surface, such as linear erosion and rock deposits. We eliminated the vegetation cover and buildings in the processing step.

Table 1. Summarized inventory of spatial variability of terrain features (types and size) according to each data source and time spent on data processing.

| Data type | Time spent (h) | | Visualized features | |
	Field survey*	Processing data**	Types	Size (m)
Topographic charts (1968)	–	Few minutes	Main drainages, large geologic contacts	Decameter or larger
RTK-GNSS	Days - weeks	Minutes	Gravitational deposits (landslides), erosion (rill, gully), geologic contacts	Meter or larger
UAV-GNSS	Few hours - days	Hours (50h 40min)	Gravitational deposits (landslides), erosion (sheet, rill, gully), anthropogenic infrastructure, vegetation	Centimeter, meter, or larger

*Depends on the size and accessibility of the site, work scale, duration of field acquisition, equipment autonomy, and weather conditions; **Depends on computer power, resolution settings, and point cloud density.

Table 2. Checkpoints (CP), altitude (m) of each checkpoint, and differences between the respective DTMs and checkpoints in meters (m) were listed by pre-existing data from nautical charts (1968), RTK-GNSS, and UAV (phantom 3).

CP	Altitude	Pre-existing data	RTK-GNSS	UAV with checkpoints
P1	53.72	-2.65	-0.18	-0.41
P2	10.82	14.66	-0.14	-0.82
P3	28.53	5.27	0	-0.49
P4	24.87	8.05	0	-0.85
P5	13.71	14.56	0.11	1.95
P6	38.84	6.45	0.11	-0.69
P7	63.31	7.01	-0.31	-0.27
P8	77.97	2.43	0.37	-0.63
P9	10.26	17.95	0.02	1.36
P10	12.29	19.62	0.12	-0.98
P11	42.93	8	0.02	0.9
P12	22.72	17.59	2.07	1.05
P13	20.82	10.87	0.01	-2.6
P14	74.50	8.97	0	0.03
P15	51.40	-1.95	-0.02	-4.92
P16	60.92	10.57	0.02	-1.85
P17	3.30	17.12	0	1.02
P18	40.77	5.75	0	-7.36
P19	14.95	10.31	-0.05	-0.93
P20	47.93	23.92	0.02	-3.27
	MAE	10.7	0.18	1.61
	RMSE	12.3	0.48	2.37
	RMSE/MAE	1.15	2.6	1.47

MAE: mean absolute error; RMSE: root mean square error.

boulder deposits — located on the ground surface, such as vegetation cover and anthropogenic infrastructure (buildings), which were eliminated for the comparative analyses of the profiles.

Spatial variability accuracy

The DTMs based on pre-existing data, RTK-GNSS, and UAV photogrammetry presented distinct spatial distribution patterns of ground features in fine-scale analysis. In the comparative assessment of 3D models with field observations, some discrepancies were detected, mainly concerning the slope curvature and the linear erosion density (see Figs. 2 and 10). The slope curvature based on pre-existing data (Fig. 10A) was divergent from the convex curvature classified in the field and hid linear erosion features. The 3D model of RTK-GNSS (Fig. 10B) elucidated a similar slope curvature but presented low linear erosion density as gullies (< 10) compared to field observations (> 20). The UAV-GNSS 3D model (Fig. 10C) represented the slope curvature of the study area more accurately. As observed in the field, the model showed a similar density of gullies (> 15).

Orthophotos: pre-existing data and UAV

The pre-existing orthophoto (2011) had a 30 cm sampling distance. It showed the landscape change processes, such as linear erosion, rock deposits, main streams, vegetation density, and occupation infrastructure (Fig. 11A). Despite the photogrammetry's centimetric accuracy, the orthophoto was limited to the spatial distribution of surface data. This gap in vertical data hinders the morphometric assessment of the landscape (e.g., elevation and slope gradient) and leads to less accurate digital models (Figs. 11B and 11C). On the other hand, the
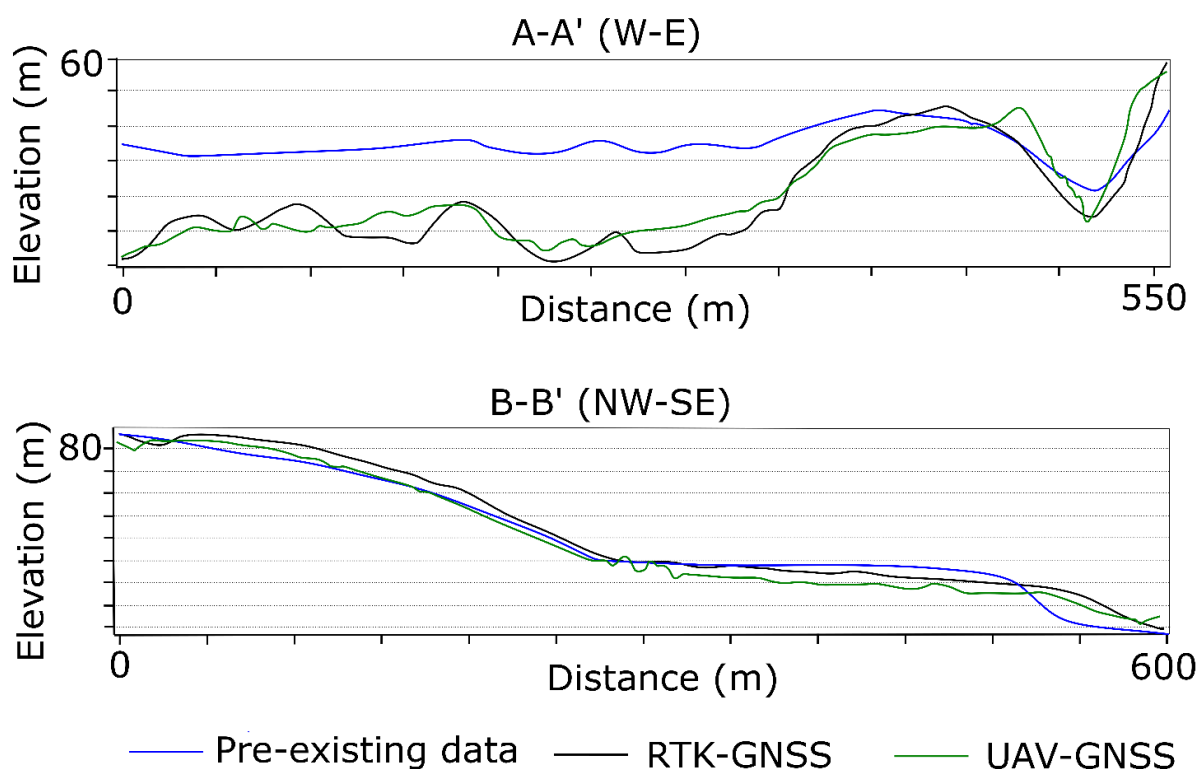

Figure 9. Comparative assessment of the topographic profiles A-A' and B-B' (see location in Fig. 8) from pre-existing data (blue), RTK-GNSS (black), and UAV-GNSS (green).

UAV orthomosaic, with a ground sampling distance of 0,0179 m (1,79 cm per px), presented consistency in the cell-by-cell continuity, satisfactorily smoothening the ground (Fig. 12). Thus, the DTM was more realistic when compared to checkpoints and field observations.

DISCUSSION

Trindade Island is part of Brazil's territory that has natural hazardous environments with human occupation (requiring geohazards assessments) and unique geology that comprises a recent volcanic landscape. So far, surface temporal data are unavailable and prevent predictive geohazard analyses. Also, reaching the island is difficult and has limited the fieldwork for most researchers. We selected a pilot area on watersheds with anthropogenic infrastructure and carried out a practical assessment of three different geospatial data sources. The main points of this study, that require discussion, are summarized below, including the accuracy issues and limitations of each technique, besides the challenges and complexities of conducting a spatial (aerial and terrestrial) survey on the Trindade Island landscape.

Pre-existent data: nautical charts and orthophoto

The pre-existing surveys included a nautical chart of DHN (1968) with 20 and 5 m interval contour lines and a 2011 photogrammetry survey with a 30 cm sampling distance. Therefore, the photogrammetry survey regarded the spatial distribution of ground features, which avoided visualizing morphometric variations, such as elevation and slope gradient. Thus, the 3D model of Trindade Island based on pre-existing data is inadequate for detailed analyses; after all, the model overgeneralizes fine-scale changes in the landscape. Such inadequacy highlights the importance of surveying data with high vertical accuracy on Trindade Island to study the terrain surface in detail.
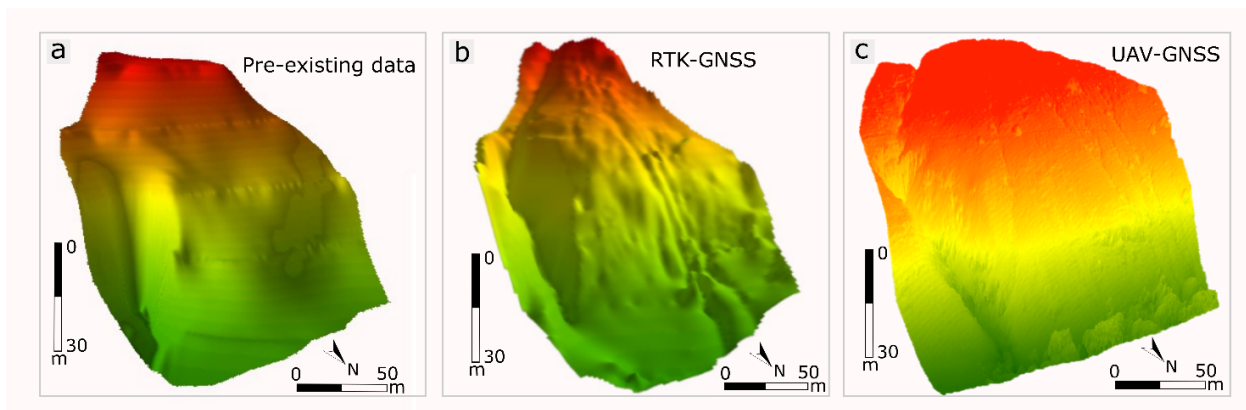

Figure 10. The selected site area to compare the 3D models generated in the GIS environment according to different techniques: (A) pre-existing topographic data of Trindade Island; (B) RTK GNSS survey; (C) UAV photogrammetry survey. The main differences are terrain curvature and terrain roughness.
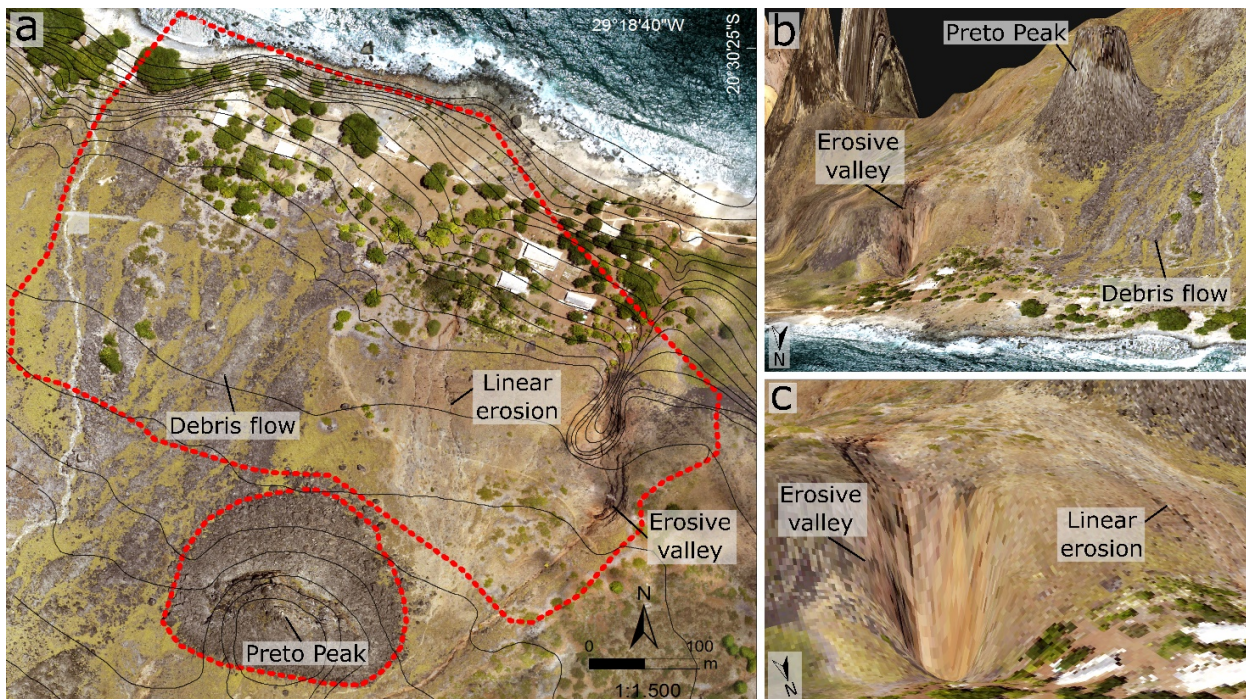

Figure 11. Geo-referenced orthophotos: (A) generated in 2011 from the pre-existing data (topographic map with contour lines 20 m-interval and orthophoto with 30cm-resolution), and the red outline refers to the study area; (B) and (C) detail of the 3D model performed from pre-existing data of Trindade Island (2x vertical exaggeration).

Whereas the topographic data of nautical charts (from 1968) are frequently used for geomorphology and geology studies on Trindade Island (e.g., Angulo *et al.* 2018, Barão *et al.* 2020, Nogueira *et al.* 2020), our results evaluate the accuracy of such data and allow discussion about the work scales that should be used. Despite the overall mean error of the DTM from pre-existing data being significantly higher than the overall mean error of the RTK-GNSS and UAV data, the profiles produced demonstrated that the vertical data were compatible with accurate methods, especially where it presents contour lines. Therefore, considering the precision of the data source and the DTM error, it is recommended to use nautical charts for regional studies on an analysis scale > 1:10,000.

RTK-GNSS: irregular data from rugged terrain

RTK-GNSS is a current technique used in different approaches due to high-accuracy positioning, such as surface mapping, relief modeling, monitoring the dynamic displacements while roving, monitoring of structures, and cadastral surveys (e.g., Gili *et al.* 2000, Sun *et al.* 2010, Im *et al.* 2013, Jin *et al.* 2014, Dabove *et al.* 2019, Mohamed *et al.* 2020).

In the present study, the DTM from RTK-GNSS data presents centimetric vertical accuracy. This accuracy is significantly higher than that of the UAV (meter) or the pre-existing data (decameter). In this regard, our comparative analyses of the interpolation procedure — in the ArcGIS software — elucidate that the interpolation method of choice is crucial. For instance, the spline method provided the DTM with the highest vertical accuracy on a centimeter scale, differently from kriging, TIN, IDW, and topo to raster. Therefore, the spline is an adequate tool for modeling irregular sampling (e.g., Lee *et al.* 1997) regarding vertical analysis — presumably due to the mathematical functions of the method (see Childs 2004, Paramasivam and Venkatramanan 2019).

Although the DTM has centimetric vertical accuracy, the spatial variability of the surface features was underestimated and limited to sizes in meters. However, we expected this result from the sampling theory point of view (e.g., Stehman 1999, De Gruijter *et al.* 2006, Gregoire and Valentine 2007, Stehman and Foody 2009, Brus *et al.* 2011), as the sampling spatial density, distribution, and frequency of our survey did not enable a spatial object with centimetric detail. This scenario regarding the RTK-GNSS application as a terrestrial method presents limitations when used on rugged terrains. In this sense, the main challenges that influenced field surveying and, consequently, post-processing, already reported by previous researchers (e.g., Roosevelt 2014, Tokura and Kubo 2017, Deng *et al.* 2019), are summarized below:

- Rugged relief and heterogeneous landscape, which limited access in the study area, resulted in an irregular grid of points cloud (Fig. 4A);
- The stony ground (roughened land surface) and higher slope led to dangerous walking (high probability of operator injury and equipment damage) (Fig. 13A);
- Large rock deposits (Fig. 13B) hindered or even impaired data acquisition resulting in a discontinuous point grid, besides the dangerous trek and the operator being required to be physically trained;
- A deep valley with large landslides (Fig. 13C) resulted in gaps in the density of points due to the impossibility of walking with the rover;
- The high density of vegetation on foot slopes (Fig. 13D) affected trekking and interfered with the satellite signal, thus reducing the accuracy of the survey.

The DTM from RTK-GNSS data is excellent for analyses requiring vertical scale accuracy, such as morphometrics studies (e.g., Brasington *et al.* 2013, Rodrigues *et al.* 2019). In the present study, considering the precision of the data source and
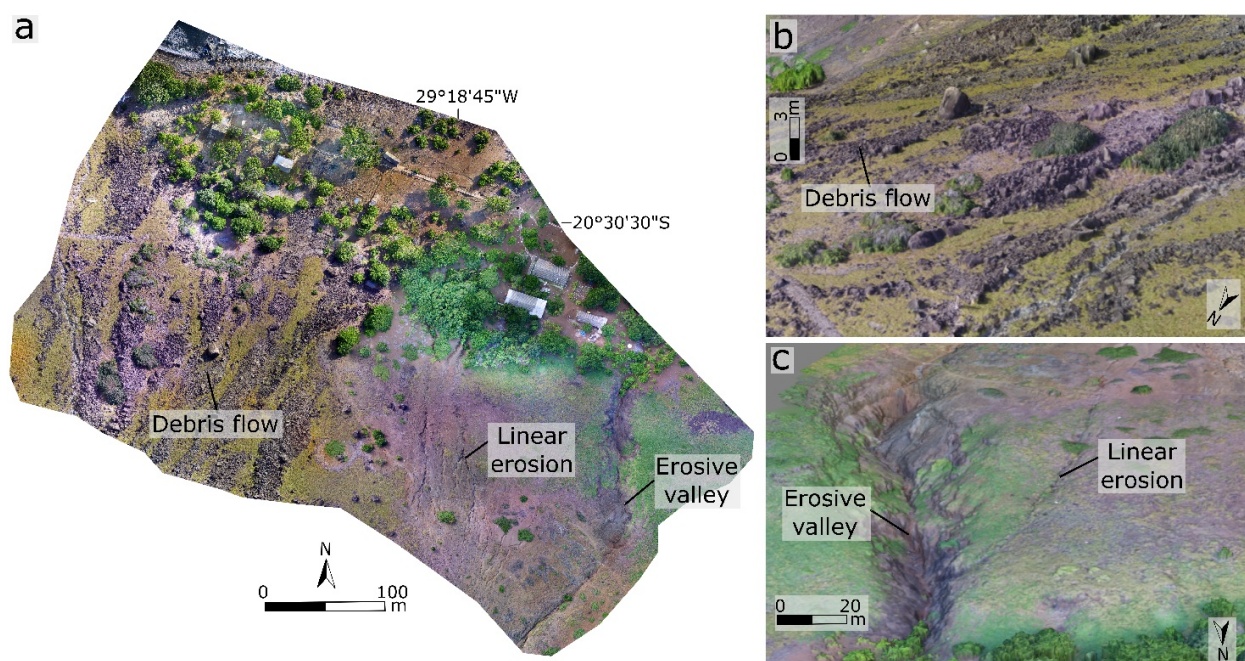

Figure 12. Geo-referenced orthophotos: (A) generated in 2019 from UAV photogrammetry (Sfm) with 1,79cm-resolution; (B and C) detail of a 3D model performed from UAV photogrammetry (Sfm) (1x vertical exaggeration).

the error of the DTM, it is recommended to use RTK-GNSS on slope surface analyses on a scale > 1:1,500. On the other hand, such data have proven to be inadequate for fine-scale investigation of spatial ground variability on landscapes with a high density of linear erosion.

UAV with high-accuracy positioning using RTK-GNSS

The UAV has an advantage over traditional data capture in mapping or monitoring applications due to high spatial and temporal resolution, besides representing a low-cost alternative to the classical crewed aircraft (Colomina *et al.* 2008, Remondino *et al.* 2011, Gonçalves and Henriques 2015).

Herein, the data quality from UAV with GCP measured by RTK-GNSS (e.g., Stempfhuber and Buchholz 2011, Mohamad *et al.* 2019) is appropriate for a detailed terrain surface inventory. In the models, the microtopography is visible, such as individual boulders, erosion, anthropogenic infrastructure, and vegetation (Fig. 7). In this sense, the high density (196 points/m^2) and homogenous survey sampling led to high spatial accuracy (Fig. 5A) (e.g., Roosevelt 2014). On the other hand, vertical accuracy was probably affected by the distribution and density of the GCPs (e.g., Martínez-Carricondo *et al.* 2018, Oniga *et al.* 2020), which was low (five per flight) and heterogeneous. Like in the RTK-GNSS survey, the data

collected from the UAV also presented challenges that influenced field acquisition time, such as:

- Scarce places on the terrain to attach the coded target, since surfaces were usually covered by large debris flow deposits or mainly formed by rock outcrops (Figs. 14A and 14B), which is complex even with natural targets;
- Sunlight reflected on the target, making it impossible for the program to recognize the code (Fig. 14C);
- Natural obstacles, such as steeply sloping hills (Fig. 14D) and large trees (Fig. 14E) in the survey area, obstructed the UAV's flight. As a result, the gap in image overlapping in the northeast of the pilot area coincided with the tallest trees zone;
- Numerous curious birds flying near the UAV created a severe risk of accidentally striking the equipment, which interfered with the survey (Fig. 14F);
- Orthomosaic gaps linked to the survey's boundaries (Figs. 14G, 14H and 14I) indicated that the survey area should be slightly larger than the actual area of interest.

From all of the above, the DTM from UAV data is excellent for analysis requiring a centimetric spatial scale, in which a detailed description of terrain features is crucial. Considering the precision of the data source and the error of the DTM, the UAV data can be used in analyses with a scale < 1:1,500.
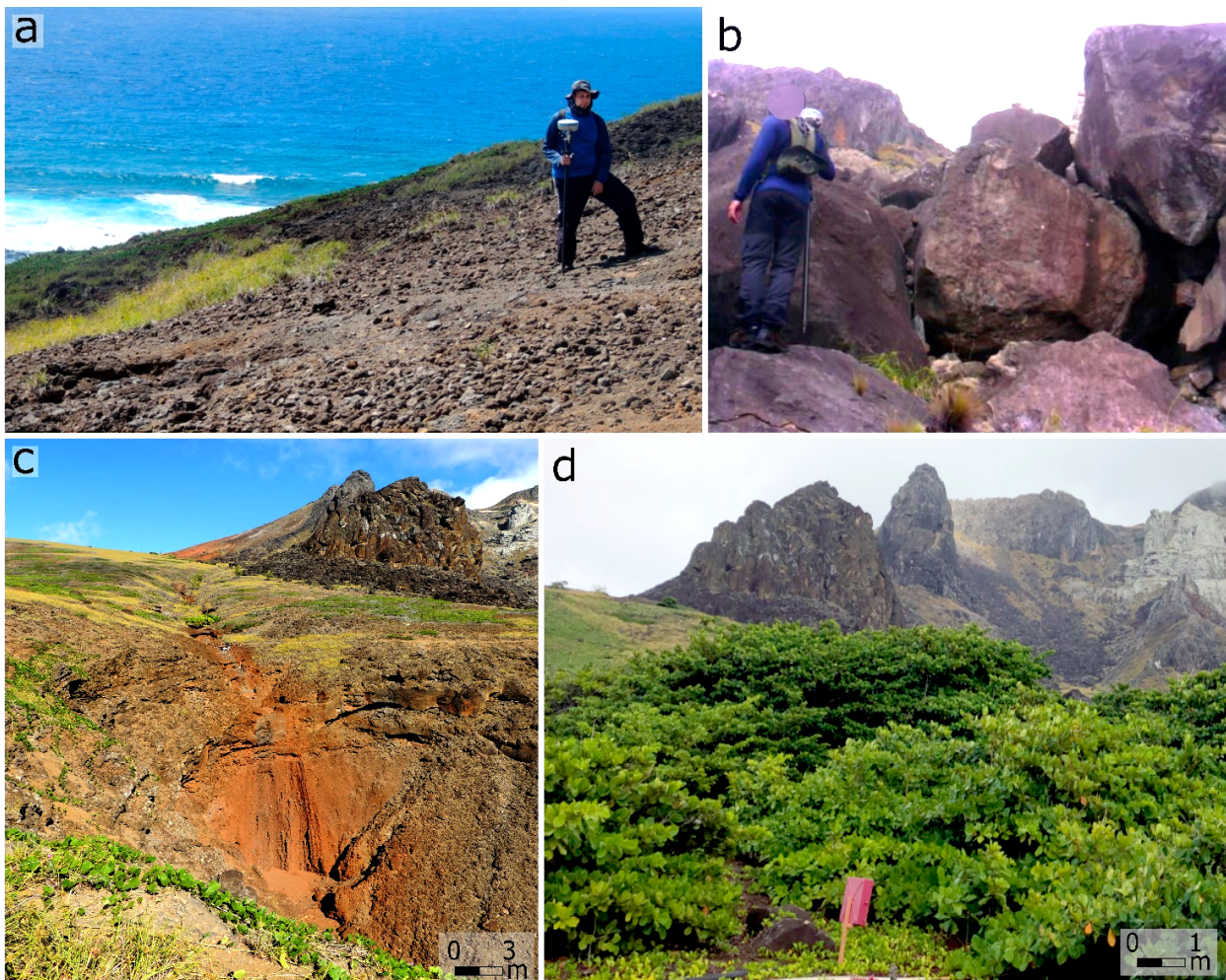

Figure 13. Challenges faced during the RTK-GNSS surveying: (A) data acquisition with rover within the static-kinematic method (stop and go) on accessible terrain and the stony ground and high slope led to dangerous walking; (B) obstacles from metric and decametric boulders, (C) deep erosive valley, and (D) vegetation density on foot slopes.
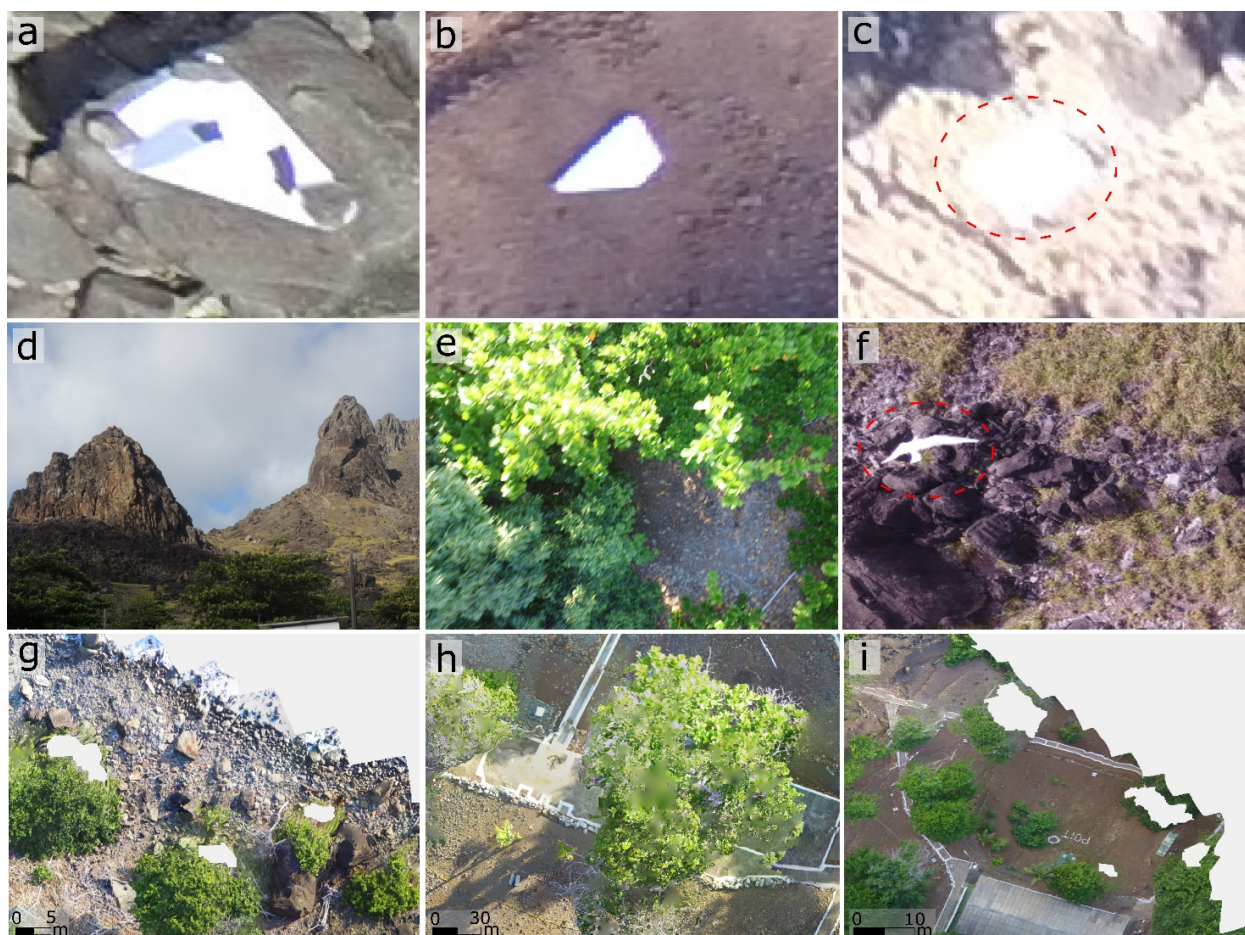
Figure 14. Issues during the UAV survey and post-processing results: (A and B) problems in finding viable places to attach the target (due to the outcropping of the rocky substrate), enabling the strong winds to flip the targets and preventing the visualization of the codes; (C) intense sun exposure may reflect on the target, making it impossible to identify the targets in the post-processing stage; (D, E and F) problems during the flight, obstacles concerning high relief, large trees, and curious birds flying close to the UAV, respectively; (G, H, and I) gaps limited to the boundaries of the survey and in regions of higher trees.

However, to access models with centimetric vertical accuracy, it is recommended to use a higher density with homogenous distribution of GPC than that used in the present study, but our results demonstrated satisfactory relief inventory.

CONCLUSIONS

This work presented a practical assessment of three geospatial data sources: nautical charts, RTK-GNSS, and UAV-GNSS collected on Trindade Island. In addition, we performed extensive data acquisition with corresponding processing to produce DTMs and an orthomosaic for relief modeling. We also demonstrated the challenges and complexity of the spatial (aerial and terrestrial) survey in remote hazardous environments with a recent volcanic landscape.

For geohazards assessment on Trindade Island, models that allow detailed visualization of specific geological data are needed, such as density and types of linear erosion, the boundary of landslides, gravitational deposits dimension, lithology differences on the surface, anthropogenic infrastructure, vegetation distribution, and morphometric parameters. In this sense, there is a need to sample data with distance, distribution, and density that enable models with high vertical and spatial accuracy.

Herein, the UAV with vertical data measured by the RTK-GNSS survey has proven to address such needs due to its sampling distance (centimetric and homogenous) and density (196 points/m^2). Additionally, the DTM with high accuracy provided a more detailed inventory than the other techniques. In summary, the UAV with the GCP technique proved to be the most viable option in isolated and difficult sites (with low vegetation cover) when compared to the RTK-GNSS, especially in terms of acquisition time and accessibility.

Despite the advantages of the UAV-GNSS application, we demonstrated that other techniques are worthwhile depending on the purpose and scale of the analysis. For instance, cartographic products, such as the nautical chart of Trindade Island, are adequate for regional studies, even more so on the island where access to conduct a field analysis is limited. Furthermore, RTK-GNSS, although not practical when used on slopes, provides a DTM with centimeter vertical accuracy, which is excellent for morphometric analysis. Finally, we encourage the authorities to conduct monitoring based on the UAV-GNSS method presented herein. Thereby, it will enable a temporal inventory and future geohazards prediction studies on Trindade Island.

ACKNOWLEDGMENTS

ARTICLE INFORMATION

REFERENCES

Abdalla A., Mustafa M. 2021. Horizontal displacement of control points using GNSS differential positioning and network adjustment, *Measurement*, **174**:108965. https://doi.org/10.1016/j.measurement.2021.108965

Aguilar F.J., Agüera F., Aguilar M.A., Carvajal, F. 2005. Effects of terrain morphology, sampling density, and interpolation methods on grid DEM accuracy. *Photogrammetric Engineering & Remote Sensing*, (7):805-816. https://doi.org/10.14358/pers.71.7.805

Almeida F.F.M. 1961. *Geologia e petrologia da ilha de Trindade*. Dissertation, Departamento Nacional de Produção Mineral, Rio de Janeiro, 197 p.

Almeida F.F.M. 2002. Ilha de Trindade: registro de vulcanismo cenozoico no Atlântico Sul In: Schobbenhaus C., Campos D.A., Queiroz E.T., Winge M. (Eds.). *Sítios geológicos e paleontológicos do Brasil*. Brasília: DNPM/CPRM – Comissão Brasileira de Sítios Geológicos e Paleobiológicos (SIGEP), p. 369-377.

Angulo R.J., Souza M.C., Barboza E.G., Rosa M.L.C.C., Fernandes L.A., Guedes C.C.F., Oliveira L.H.S., Manzolli R.P., Disaró S.T., Ferreira A.G., Martin C.M. 2018. Quaternary sea-level changes and coastal Evolution of the Island of Trindade, Brazil. *Journal of South American Earth Sciences*, **84**:208-222. https://doi.org/10.1016/j.jsames.2018.04.003

Barão L.M., Trzaskos B., Angulo R.J., Souza M.C., Daufenbach H.F., Santos F.A., Vasconcellos E.M.G. 2020. Deformational structures developed in volcanic sequences as a product of tectonic adjustments in the South Atlantic Ocean. *Journal of South American Earth Sciences*, **104**:102812. https://doi.org/10.1016/j.jsames.2020.102812

Brasington J., Langham J., Rumsby B. 2003. Methodological sensitivity of morphometric estimates of coarse fluvial sediment transport. *Geomorphology*, **53**(3-4):299-316. https://doi.org/10.1016/S0169-555X(02)00320-3

Brus D.J., Kempen B., Heuvelink G.B.M. 2011. Sampling for validation of digital soil maps. *European Journal of Soil Science*, **62**(3):394-407. https://doi.org/10.1111/j.1365-2389.2011.01364.x

Cavalcanti I.F.A, Ferreira N.J., Silva M.G.A.J., Dias M.A.F. 2009. *Tempo e clima no Brasil*. São Paulo: Oficina de Textos.

Chaudhry M.H., Ahmad A., Gulzar Q., Farid M.S., Shahabi H., Al-Ansari N. 2021. Assessment of DSM based on radiometric transformation of UAV data. *Sensors*, **21**(5):1649. https://doi.org/10.3390/s21051649

Childs C. 2004. Interpolating surfaces in ArcGIS spatial analyst. *ArcUser*, **3235**(569):32-35.

Colomina I., Blázquez M., Molina P., Parés M.E., Wis M. 2008. Towards a new paradigm for high-resolution low-cost photogrammetry and remote sensing. *IAPRS&SIS*, p. 1201-1206.

Dabove P. 2019. The usability of GNSS mass-market receivers for cadastral surveys considering RTK and NRTK techniques. *Geodesy and Geodynamics*, **10**(4):282-289. https://doi.org/10.1016/j.geog.2019.04.006

De Gruijter J., Brus D.J., Bierkens M.F.P., Knotters M. 2006. *Sampling for natural resource monitoring*. Berlin: Springer, 332 p.

Deng F., Rodgers M., Xie S., Dixon T.H., Charbonnier S., Gallant E.A., Vélez C.M.L., Ordoñez M., Rocco M., Voss N.K., Richardson J.A. 2019. A High-resolution DEM generation from spaceborne and terrestrial remote sensing data for improved volcano hazard assessment - A case study at Nevado del Ruiz, Colombia. *Remote Sensing of Environment*, **233**:111348. https://doi.org/10.1016/j.rse.2019.111348

Diretoria de Hidrografia e Navegação (DHN). 1971. Carta náutica Ilha da Trindade n. 21, escala 1:15,000 e escala 1:5,000. DHN.

Evans M., Lindsay J. 2010. High resolution quantification of gully erosion in upland peatlands at the landscape scale. *Earth Surface Processes and Landforms*, **35**(8):876-886. https://doi.org/10.1002/esp.1918

Gili J.A., Corominas J., Rius J. 2000. Using global positioning system techniques in landslide monitoring. *Engineering Geology*, **55**(3):167-192. https://doi.org/10.1016/S0013-7952(99)00127-1

Global Volcanism Program. 2013. Volcanoes of the World. *In*: Venzke E. (Ed.). *Smithsonian Institution v. 4.7.5*. Available at: https://volcano.si.edu/volcano.cfm?vn=342110. Accessed on: Feb. 10, 2020.

Gonçalves J.A., Henriques R. 2015. UAV photogrammetry for topographic monitoring of coastal areas. *ISPRS Journal of Photogrammetry and Remote Sensing*, **104**:101-111. https://doi.org/10.1016/j.isprsjprs.2015.02.009

Gregoire T.G., Valentine H.T. 2007. *Sampling strategies for natural resources and the environment*. Boca Raton: CRC Press, 496 p.

Guenzi D., Allasia P., Baldo M., Giordan D. 2019. Open source, low-cost and modular fixed-wing UAV with BVLOS flight capabilities for geohazards monitoring and surveying. *IEEE 5th International Workshop on Metrology for*

AeroSpace (MetroAeroSpace). Torito, p. 160-164. https://doi.org/10.1109/MetroAeroSpace.2019.8869630

Haala N., Cramer M., Weimer F., Trittler M. 2011. Performance test on UAV-based photogrammetric data collection. *In*: *International Archives of the Photogrammetry, Remote Sensing and Spatial Information Sciences*, **38**(6):7-12.

Hashemi-Beni L., Jones J., Thompson G., Johnson C., Gebrehiwot A. 2018. Challenges and opportunities for UAV-based digital elevation model generation for flood-risk management: a case of Princeville, North Carolina. *Sensors*, **18**(11):3843. https://doi.org/10.3390/s18113843

Hu X., Hu K., Zhang X., Wei L., Tang J. 2019. Quantitative assessment of the impact of earthquake-induced geohazards on natural landscapes in Jiuzhaigou Valley. *Journal of Mountain Science*, **16**(2):441-452. https://doi.org/10.1007/s11629-018-5240-7

Im S.B., Hurlebaus S., Kang, Y.J. 2013. Summary review of GPS technology for structural health monitoring. *Journal of Structural Engineering*, **139**(10):1653-1664. https://doi.org/10.1061/(asce)st.1943-541x.0000475

Jin S., Cardellach E., Xie F. 2014. *GNSS remote sensing*. Dordrecht: Springer, 276 p.

Karunasingha D.S.K. 2022. Root mean square error or mean absolute error? Use their ratio as well. *Information Sciences*, **585**:609-629. https://doi.org/10.1016/j.ins.2021.11.036

Lee S., Wolberg G., Shin, S.Y. 1997. Scattered data interpolation with multilevel B-splines. *IEEE Transactions on Visualization and Computer Graphics*, **3**(3):228-244. https://doi.org/10.1109/2945.620490

Marinha do Brasil. 2011. *Imagem Aérea, escala 1:10.000*. Brasil: Marinha do Brasil.

Martínez-Carricondo P., Agüera-Vega F., Carvajal-Ramírez F., Mesas-Carrascosa F.J., García-Ferrer A., Pérez-Porras F.J. 2018. Assessment of UAV-photogrammetric mapping accuracy based on variation of ground control points. *International Journal of Applied Earth Observation and Geoinformation*, **72**:1-10. https://doi.org/10.1016/j.jag.2018.05.015

Mendez-Astudillo J., Lau L., Tang Y.T., Moore T. 2021. A new Global Navigation Satellite System (GNSS) based method for urban heat island intensity monitoring. *International Journal of Applied Earth Observation and Geoinformation*, **94**:102222. https://doi.org/10.1016/j.jag.2020.102222

Mohamad N., Khanan M.F.A., Ahmad A., Din A.H., Shahabi H. 2019. Evaluating water level changes at different tidal phases using UAV photogrammetry and GNSS vertical data. *Sensors*, **19**(17):3778. https://doi.org/10.3390/s19173778

Mohamed E.A., Albert Y.G., Amr E.M. 2020. Improving the Accuracy of RTK-GNSS Data in Digital Elevation Model. *Proceedings of the 2020 3rd International Conference on Geoinformatics and Data Analysis*, 86-90.

Mohammadi A., Karimzadeh S., Jalal S.J., Kamran K.V., Shahabi H., Homayouni S., Al-Ansari N. 2020. A multi-sensor comparative analysis on the suitability of generated DEM from Sentinel-1 SAR interferometry using statistical and hydrological models. *Sensors*, **20**(24):7214. https://doi.org/10.3390/s20247214

Muço B., Alexiev G., Aliaj S., Elezi Z., Grecu B., Mandrescu N., Milutinovic Z., Radulian M., Ranguelov B., Shkupi, D. 2012. Geohazards assessment and mapping of some Balkan countries. *Natural Hazards*, **64**(2):943-981. https://doi.org/10.1007/s11069-012-0185-6

Nogueira G.S., Effgen J.F., Marchioro E. 2020. Análise morfométrica e morfológica da Ilha da Trindade, Atlântico Sul, Brasil. *Sociedade & Natureza*, **32**:222-248. https://doi.org/10.14393/SN-v32-2020-49647

Oniga V.E., Breaban A.I., Pfeifer N., Chirila C. 2020. Determining the suitable number of ground control points for UAS images georeferencing by varying number and spatial distribution. *Remote Sensing*, **12**(5):876. https://doi.org/10.3390/rs12050876

Paramasivam C.R., Venkatramanan S. 2019. An introduction to various spatial analysis techniques *In*: Chung S.Y., Venkatramanan S., Viswanathan P.M. (Eds.). *GIS and geostatistical techniques for groundwater science*. Amsterdam: Elsevier, p. 23-30.

Pedroso D., Panisset J.S., Abdo L.B.B. 2017. Climatologia da Ilha da Trindade. In: Campos T.A.S. (Ed.). *Protrindade:* programa de pesquisas científicas na Ilha da Trindade 10 anos de pesquisas. Brasília: Secretaria da Comissão Interministerial para os Recursos do Mar, p. 27-34.

Ramos A.M., Hasegawa J.K., Tommaselli A.M.G., Galo M., Henrique B.S.A. 2008. Emprego de fotogrametria digital com imagens coletadas por helicópteros em apoio à determinação de linhas de base das Ilhas Martim Vaz. *II Simpósio Brasileiro de Ciências Geodésicas e Tecnologias da Geoinformação*, p. 8-11.

Remondino F., Barazzetti L., Nex F., Scaioni M., Sarazzi D. 2011. UAV photogrammetry for mapping and 3d modeling–current status and future perspectives. *International archives of the photogrammetry, Remote Sensing and Spatial Information Sciences*, **38**(1):25-31. https://doi.org/10.5194/isprsarchives-XXXVIII-1-C22-25-2011

Rodrigues G.S., Oliveira U.R, Albuquerque M.G., Antiqueira J.A. 2019. Variabilidade topográfica do sistema praiaduna em balneários da costa central e sul do Rio grande do sul utilizando rtk-gps. *In*: Roque A.C., Paula D.P., Dias J.A., Fonseca L.C., Rodrigues M.A.C., Albuquerque M.G., Pereira S.D. (Eds.). *Saindo da zona de conforto:* a interdisciplinaridade das zonas costeiras. Tomo VIII da Rede BRASPOR. Rio de Janeiro: FGEL-UERJ, p. 239-253.

Roosevelt C.H. 2014. Mapping site-level microtopography with real-time kinematic global navigation satellite systems (RTK GNSS) and unmanned aerial vehicle photogrammetry (UAVP). *Open Archaeology*, **1**:29-53. https://doi.org/10.2478/opar-2014-0003

Santos R., Quartau R., Silveira A.B., Ramalho R., Rodrigues A. 2019. Gravitational, erosional, sedimentary and volcanic processes on the submarine environment of Selvagens Islands (Madeira Archipelago, Portugal). *Marine Geology*, **415**:105945. https://doi.org/10.1016/j.margeo.2019.05.004

Silva N.G., Alves R.J.V. 2017. Plantas vasculares terrestres da Ilha da Trindade. *In*: Campos T.A.S. (Ed.). *Protrindade:* programa de pesquisas científicas na Ilha da Trindade 10 anos de pesquisas. Brasília: Secretaria da Comissão Interministerial para os Recursos do Mar, p. 195-198.

Souza Filho C.R., Crósta A.P. 2003. Geotecnologias aplicadas à Geologia. *Revista Brasileira de Geociências*, **33**(2):1-4.

Stehman S.V. 1999. Basic probability sampling designs for thematic map accuracy assessment. *International Journal of Remote Sensing*, **20**(12):2423-2441. https://doi.org/10.1080/014311699212100

Stehman S.V., Foody G.M. 2009. Accuracy assessment. *In*: Warner T.A., Foody G.M., Nellis M.D. (Eds.). *The SAGE handbook of remote sensing*. London: SAGE, p. 297-309.

Stempfhuber W., Buchholz M. 2011. A precise, low-cost RTK GNSS system for UAV applications. *International Archives of the Photogrammetry, Remote Sensing and Spatial Information Sciences – ISPRS*, **38**:1/C22.

Sun H., Slaughter D.C., Ruiz M.P., Gliever C., Upadhyaya S.K., Smith, R.F. 2010. RTK GPS mapping of transplanted row crops. *Computers and Electronics in Agriculture*, **71**(1):32-37. https://doi.org/10.1016/j.compag.2009.11.006

Tan Q., Bai M., Zhou P., Hu J., Qin X. 2021. Geological hazard risk assessment of line landslide based on remotely sensed data and GIS. *Measurement*, **169**:108370. https://doi.org/10.1016/j.measurement.2020.108370

Tannant D.D. 2015. Review of photogrammetry-based techniques for characterization and hazard assessment of rock faces. *International Journal of Georesources and Environment-IJGE*, **1**(2):76-87. https://doi.org/10.15273/ijge.2015.02.009

Tokura H., Kubo N. 2017. Efficient satellite selection method for instantaneous RTK-GNSS in challenging environments. *Transactions of the Japan Society for Aeronautical and Space Sciences*, **60**(4):221-229. https://doi.org/10.2322/tjsass.60.221

United Nations Educational, Scientific and Cultural Organization (UNESCO). 2019. Geohazard Risk Reduction. UNESCO Natural Sciences Web. Available at: http://www.unesco.org/new/en/natural-sciences/special-themes/disaster-risk-reduction/geohazard-risk-reduction/. Accessed on: Jan. 10, 2020.

Uysal M., Toprak A.S., Polat N. 2015. DEM generation with UAV Photogrammetry and accuracy analysis in Sahitler hill. *Measurement*, **73**:539-543. https://doi.org/10.1016/j.measurement.2015.06.010

Wernette P., Lehner J., Houser C. 2020. What is 'real'? Identifying erosion and deposition in context of spatially-variable uncertainty. *Geomorphology*, **355**:107083. https://doi.org/10.1016/j.geomorph.2020.107083